Materials Physics and Mechanics. 2023;51(7): 34-41
Research article
http://dx.doi.org/10.18149/MPM.5172023_5

Submitted: November 12, 2023
Approved: November 30, 2023
Accepted: December 14, 2023

Toughening of nanocrystalline alloys due to grain boundary segregations: finite element modeling

A.G. Sheinerman [1] ✉, R.E. Shevchuk [2]

[1] Institute for Problems of Mechanical Engineering RAS, St. Petersburg, Russia

[2] JSC "I.I. Polzunov Scientific and Development Association on Research and Design of Power Equipment", St. Petersburg, Russia

✉ asheinerman@gmail.com

Abstract. We propose a two-dimensional (2D) model that describes toughening of nanocrystalline metallic alloys due to grain boundary (GB) segregations. Within the model, brittle GB segregations lead to the formation of satellite GB cracks near the tip of the main crack. These cracks affect the stress concentration in the vicinity of the main crack tip and lead to toughening. We performed 2D finite element simulations of crack growth in a representative volume that incorporates GB fragments without segregations and with segregations. In these simulations, GBs are modeled as interface elements, and the effect of GB segregations manifests itself in a strong reduction of the cohesive strength of these elements. We demonstrate that GB segregations in nanocrystalline alloys can increase the fracture energy and thereby toughen these solids.
Keywords: nanocrystalline alloys; grain boundaries; segregations; toughening

Acknowledgements. *The work was supported by the Russian Science Foundation (project 22-21-00056).*

Citation: Sheinerman AG, Shevchuk RE. Toughening of nanocrystalline alloys due to grain boundary segregations: finite element modeling. *Materials Physics and Mechanics*. 2023;51(7): 34-41. DOI: 10.18149/MPM.5172023_5.

Introduction

The unique mechanical properties of nanocrystalline metallic materials, such as ultrahigh strength, have made them a subject of intensive research last years (see, e.g., reviews [1-6]). Of special interest are nanocrystalline alloys with grain boundary (GB) segregations, which make these nanocrystalline solids stable against grain growth [7-11]. In addition, GB solute segregations can affect the mechanical properties of nanocrystalline alloys, including their strength, hardness and fracture toughness. For example, experiments [12-14] indicate that GB segregations can dramatically increase strength and hardness of nanocrystalline alloys. An improvement of these mechanical properties was explained by the action of various mechanisms, such as inactivation of GB dislocation sources [15-17], resistance to dislocation propagation across grains [18], and suppression of GB sliding [17,19].

In parallel with strength and hardness, GB segregations in nanocrystalline alloys influence the fracture toughness of these alloys. Since such segregations are commonly brittle, they can in some cases reduce the fracture toughness of nanocrystalline alloys [20-22]. Meanwhile, recent experiments [22] demonstrated the possibility of increasing the fracture

Publisher: Peter the Great St. Petersburg Polytechnic University

toughness and ductility of nanocrystalline Pt-Au alloys due to the formation of segregations. In these experiments, GB segregations of Au increased toughness at moderate (5 at. %) Au concentration and reduced it at high (10 at. %) Au concentration. The toughening associated with the GB segregations of Au was related [22] to the formation of secondary nanocracks at GBs containing brittle GB segregations.

Also, recent two-dimensional (2D) finite element (FE) simulations [23] of crack advance along grain or interphase boundaries that form a two-dimensional hexagonal lattice within an elastic–viscoplastic constitutive model demonstrated the possibility of fracture toughness enhancement at a moderate (up to 10-40 %) fraction of brittle boundaries followed by a drop of fracture toughness at a higher fraction of such boundaries. The toughening associated with brittle boundaries was attributed [23] to the combination of various toughening mechanisms, such as crack deflection, crack branching, the formation of secondary cracks and enhanced plastic deformation near the crack tip. However, the contributions of separate toughening mechanisms to the fracture toughness enhancement were not evaluated. Also, other FE simulations studied similar effects of toughening [24‑29] associated with the structural inhomogeneities, such as bimodal grain size distribution [24], the formation of elongated grains [25], or inhomogeneous residual stresses [27].

More recently, the contribution of crack deflection to the fracture toughness of nanocrystalline alloys with GB segregations has been theoretically studied within a 2D analytical model [30]. It appeared [30] that crack deflection can increase the fracture toughness by up to 30–35 %, and the maximum toughening is achieved if segregations are very brittle and occupy a moderate proportion of GBs. The aim of the present paper is to reveal the effects of secondary (satellite) nanocracks formed near the tip of the main crack due to the presence of brittle GB segregations on the fracture energy and toughness of nanocrystalline alloys. In the following, we suggest a 2D model that describes the toughening effect of the satellite nanocracks and describe the results of our FE simulations of the fracture energy of nanocrystaline alloys with GB segregations.

Model

Consider the effect of GB segregations on the fracture energy and toughness of nanocrystalline alloys. To do so, within our 2D model, we examine a bar of infinite length and a rectangular cross section under the plane strain state and introduce a precrack with the initial half-length l_0=0.4 μm, which is much smaller than the dimensions of the bar (Fig. 1). The bar is supposed to be loaded by a tensile load that corresponds to specified constant displacements at the upper and lower boundaries, and the direction of the initial crack is assumed to be normal to the direction of the applied load (Fig. 1). A symmetry condition is set on the left boundary of the bar, that is, the displacement in the direction normal to the boundary is prohibited, and the right boundary is assumed to be free. The displacements at the upper and lower boundaries are set small enough to prevent the cracking of GBs far from the crack tip, and the material is assumed to be linearly elastic and elastically isotropic.

In the vicinity of the tip of the initial crack, on the way of its further advance during the bar tension, there is a region simulating the grain structure. In order to reduce computational costs, the rest of the bar far from the crack tip is modeled as a homogeneous material, due to the relatively low influence of this region on the critical parameters of crack growth.

To generate a representative volume of the grain structure with the size Δa_{max}=0.4 μm located near the precrack tip, algorithms were used to construct a Voronoi diagram. The characteristic average grain width is assumed to be 50 nm, which corresponds to the experimental values for the nanocrystalline Pt-Au alloy with GB segregations [22].

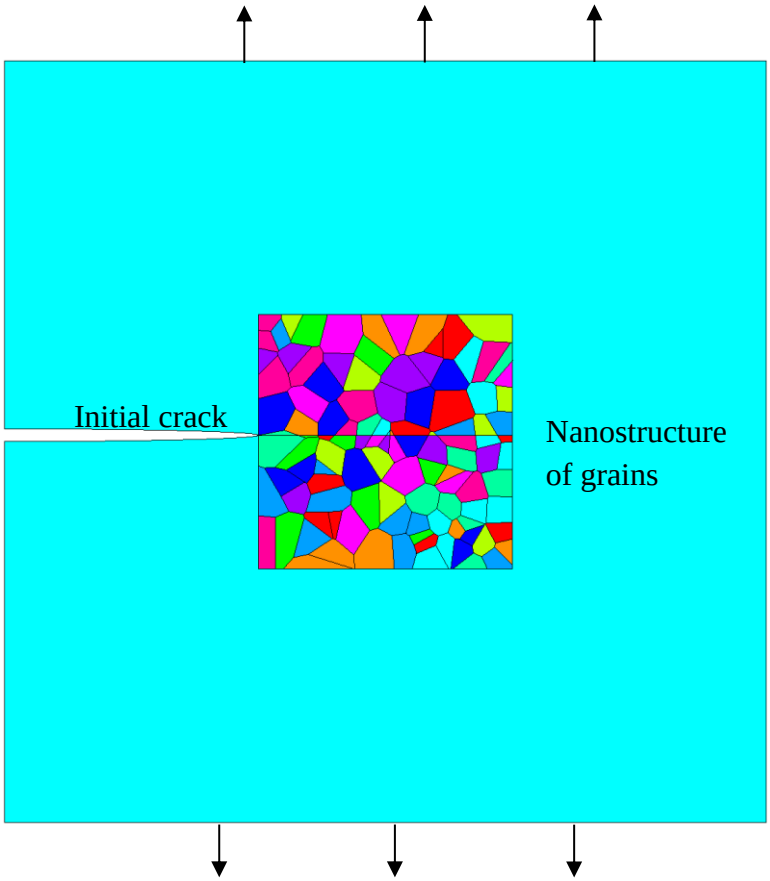

Fig. 1. Finite element model in the region near the initial crack tip, containing a nanostructure of grains

All calculations were performed in the ANSYS FE analysis system. The Young modulus E and Poisson's ratio ν of the solid were put equal to the characteristic values of those for the Pt-10Au (at. %) nanocrystalline alloy examined in [22]: E=145 GPa, ν=0.4 [31]. To construct a computational model of grains and a homogeneous region of the bar, flat elements in the plane strain state were used. To increase the accuracy of numerical calculations, when constructing a finite element mesh, finite elements with a quadratic function for approximating the displacements were used.

For simplicity, here we do not consider the effect of crack deflection on fracture toughness (assuming that the initial crack stays flat during growth) and focus on the effect of the secondary nanocracks at GBs (whose formation near the precrack tip is enhanced due to the presence of brittle GB segregations) on the growth of the initial crack. To simulate the formation of nanocracks at GBs as well as the growth of the initial crack, we define interface elements of the CZM (cohesive zone model) type at GBs and on the extension of the main crack; in the unloaded state, their thickness is equal to zero. During loading of the bar, the interface elements are elastically deformed along with the grains, and when the jump of displacements exceeds a critical value, they fracture.

The interface elements divide two contacting surfaces and are characterized by the surface potential that describes the additional total energy of the surfaces (per their unit area) associated with their separation and sliding. The surface potential φ is defined in the form originally proposed in [32] as

$$\varphi(\delta_n, \delta_t) = e\sigma_{max}\bar{\delta}_n\left[1 - (1 + \Delta_n)e^{-\Delta_n}e^{-\Delta_t^2}\right], \quad (1)$$

where $\Delta_n = \delta_n/\bar{\delta}_n$, $\Delta_t = \delta_t/\bar{\delta}_t$, σ_{max} is cohesive strength of the interface, δ_n and δ_t are the normal and tangential jumps of displacements at the interface element, respectively, and $\bar{\delta}_n$ and $\bar{\delta}_t$ are parameters. The maximum value of the surface potential $\varphi_{max} = \varphi(\delta_n \to \infty, \delta_t) = e\sigma_{max}\bar{\delta}_n$ corresponds to the specific work of normal separation of the two surfaces. The surface potential $\varphi(\delta_n, \delta_t)$ decreases with the normal separation δ_n at $\delta_n > \bar{\delta}_n$. This implies that once the relation $\delta_n > \bar{\delta}_n$ is satisfied, the contacting surfaces are energetically favored to be separated, and thus, the fracture at an interface element occurs in the region where $\delta_n > \bar{\delta}_n$. We put $\bar{\delta}_n$ = 1 nm, $\bar{\delta}_t$ = 2 nm.

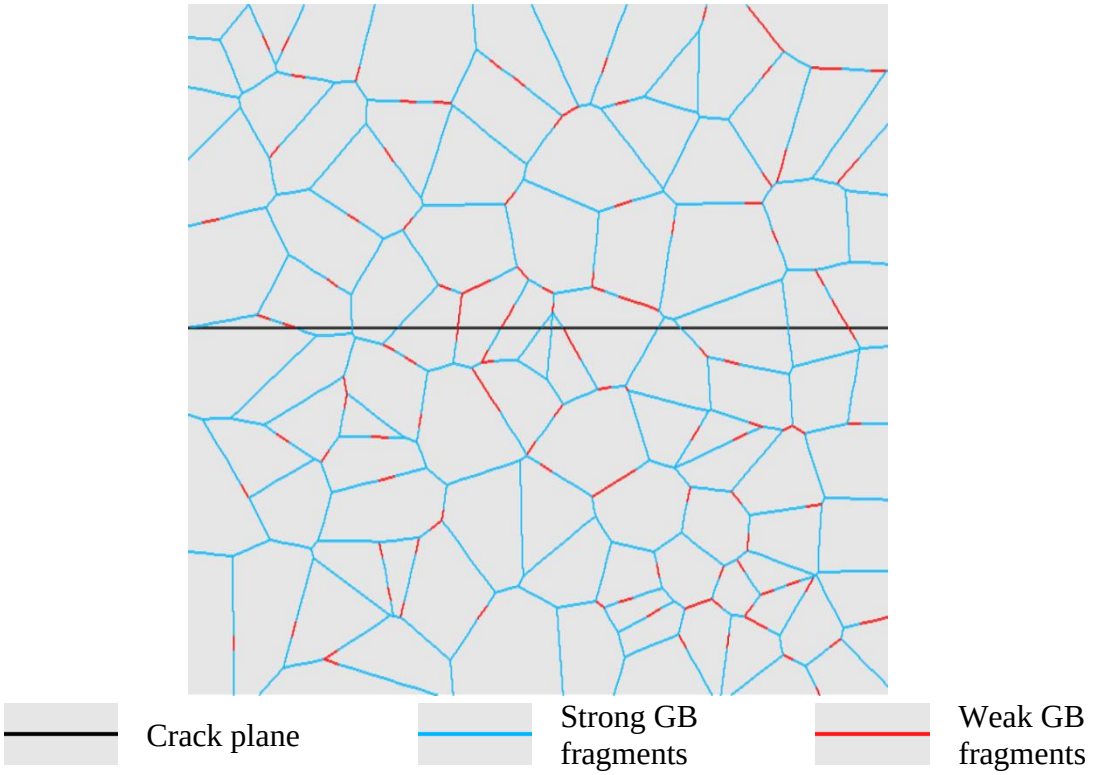

Fig. 2. The geometry of strong and weak GB fragments in the representative volume

GB segregations in the grain structure are modeled as interface elements with a strongly reduced cohesive strength σ_{max} (see Fig. 2). Focusing on the case where the fragments of GBs with segregations are very brittle, we set the value σ_{max} for the "weak" interface elements (that model GB segregations) to be 5 times smaller than that for "strong" interface elements (without GB segregations).

Let us denote the proportion c of weak GB fragments (containing GB segregations) as the ratio of the total length of weak GB fragments to the total length of GBs in the representative volume. The location of weak GB fragments is chosen randomly depending on their proportion c. Figure 2 illustrates one of the possible arrangements of strong and weak GB fragments for the case c = 15 %.

The simulation of main crack growth was carried out as follows. The bar is loaded using kinematic boundary conditions, and thus the initial stress field appears in the bar. Then, sequentially, element by element, the interface elements that make up the region in which the main crack propagates are removed. During the growth of the main crack, the interface elements in GBs can be destroyed when the critical parameters (the jumps of displacements at the elements) exceed critical values, and, thus, new nanocracks can form. The removal of interface elements was carried out using the Ekill method, which reduces the stiffness of the

required final element to a negligible value. Each step of the solution is recorded, and at all iterations of the numerical solution the value of the strain energy E, which is released during the growth of the main crack, is calculated. The magnitude of the specified displacements at the upper and lower boundaries is fixed, and so a change in the strain energy can only be caused by an increase in the length of the main crack, as well as by the formation of new nanocracks at GBs. The energy release rate G in the course of main crack growth is given by $G = -dE/da$, where a is the crack length.

Results

Figure 3 plots the dependences of the energy release rate G on the crack length increment Δa within the representative volume at various proportions c of weak GB fragments, calculated for some random configurations. The reason for the sharp decrease of the parameter G as the crack tip penetrates into the heterogeneous region and its increase as the crack exits the heterogeneous region is the formation of GB nanocracks as the main crack grows. The non-monotonic character of the curves in Fig. 3 in the interval $0.12 < \Delta a < 0.32$ μm is related to the approaching the main crack tip to GB nanocracks or moving it away from such nanocracks.

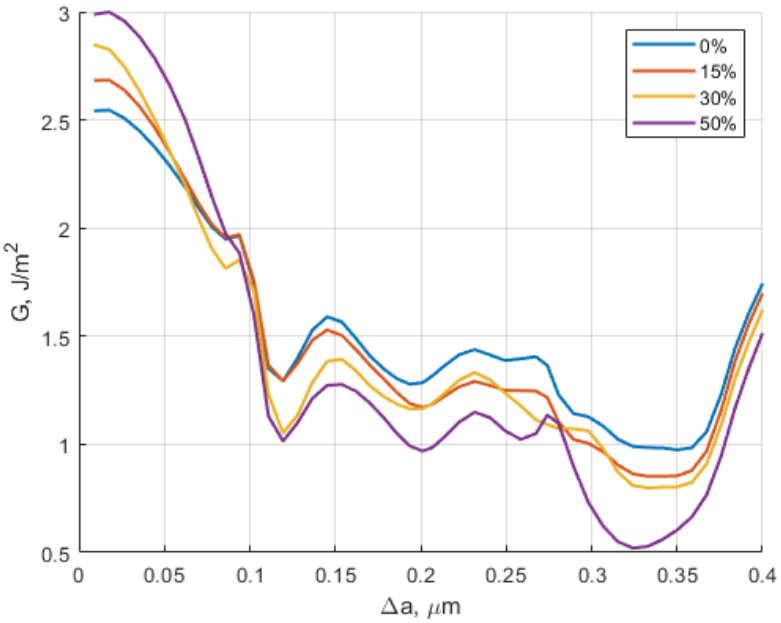

Fig. 3. Energy release rate G as a function of crack length increment Δa, for various values of the proportion c of weak GB fragments

In the absence of GB nanocracks, the critical condition for main crack growth has the form $G = G_{c0}$, where G_{c0} is the intrinsic fracture energy, which is determined by the surface energy of the solid. On the other hand, to a remote observer, the crack advances in a homogeneous medium and is characterized by the energy release rate G_0 that depends on the applied load and the crack length. Macroscopically, the crack growth condition has the form $G_0 = G_c$, where G_c is the effective fracture energy that accounts for the effect of GB nanocracks. As a result, when the energy release rate G is close to the intrinsic fracture energy G_{c0}, we have: $G_c / G_{c0} = G_0 / G$. To calculate the fracture toughness associated with crack growth over strong and weak GBs, we will consider the strongest GB along which crack propagation is most difficult and calculate the fracture energy as $G_c = \max\{(G_0 / G)G_{c0}, l_0 \le a \le l_0 + \Delta a_{\max}\}$.

Using such a calculation procedure, the fracture energy G_c was calculated for c = 0, 15, 30 and 50 %. Due to the influence of the random location of weak GB fragments on the results obtained, for each value of c, the values of the fracture energy G_c were averaged for 10 different arrangements of weak GB fragments. In this case, the geometry of GBs remains unchanged, and only the location of weak GBs varies.

Figure 4 shows the normalized fracture energy $G_c / G_c(c = 0)$ for different proportions c of weak GB fragments. It is seen in Fig. 4 that fracture energy increases with c, and for c = 50 %, an increase in the fracture energy is around 18 %. Since the fracture energy G_c is proportional to the squared fracture toughness, K_{IC}^2, this corresponds to an increase in the fracture toughness by approximately 9 %. This implies that the formation of nanocracks at weak GBs with segregations can toughen nanocrystalline alloys and the maximum fracture toughness can be achieved when the proportion of GBs with segregations is sufficiently high. At the same time, the proportion of GBs with segregations should not exceed the values at which such brittle boundaries form clusters leading to catastrophic fracture.

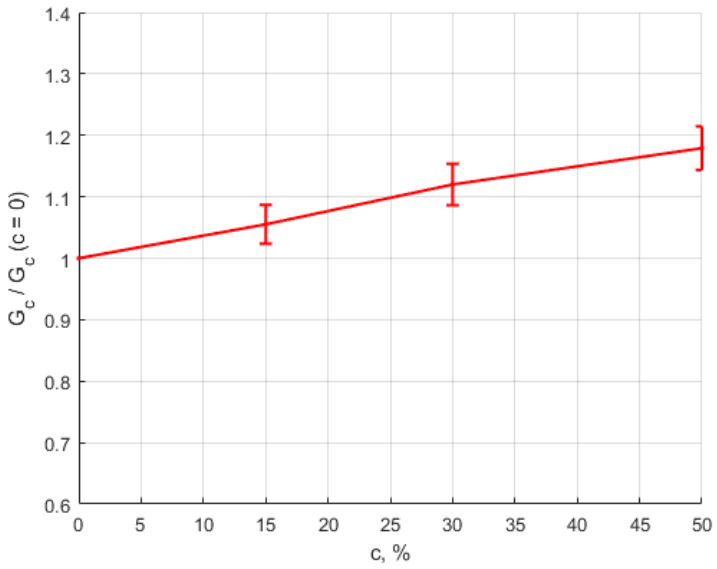

Fig. 4. Normalized fracture energy $G_c / G_c(c = 0)$ vs the proportion c of weak GB fragments

Concluding remarks

Thus, in the present paper, we have proposed a 2D model that describes the toughening due to GB solute segregations in nanocrystalline alloys. Within the model, we focused on the toughening associated with the formation of GB nanocracks at the sites for GB segregations near the tip of the main crack. These nanocracks affect the growth of the main crack and can lead to toughening. The toughening associated with the GB nanocracks is not high. For the case where GB segregations occupy 50 % of the total GB length, the fracture energy increases due to GB segregations by 18 %, which corresponds to 9 % increase in fracture toughness. However, together with other toughening mechanisms, such as crack deflection [23,30] and crack branching [23], a high enough proportion of GB segregations can considerably toughen nanocrystalline alloys [23,30]. The model is valid for the case where the fraction of the GB segregations does not exceed the values at which such brittle GBs form clusters leading to catastrophic fracture. The results of the model correlate with the experimental observations [22] of Pt-Au alloys, where GB segregations of Au led to toughening.

References

1. Meyers MA, Mishra A, Benson DJ. Mechanical properties of nanocrystalline materials. *Progr. Mater. Sci.* 2006;51: 427–556.
2. Ovid'ko IA, Valiev RZ, Zhu YT. Review on superior strength and enhanced ductility of metallic nanomaterials. *Progr. Mater. Sci.* 2018;94: 462–540.
3. Haché M, Cheng C, Zou Y. Nanostructured high-entropy materials. *J. Mater. Res.* 2020;35: 1051–1075.
4. Kushwaha AK, John M, Misra M, Menezes PL. Nanocrystalline materials: Synthesis, characterization, properties, and applications. *Crystals*. 2021;11: 1317.
5. Li H, Wang P, Wen C. Recent progress on nanocrystalline metallic materials for biomedical applications. *Nanomaterials*. 2022;12: 2111.
6. Valiev RZ, Straumal B, Langdon TG. Using severe plastic deformation to produce nanostructured materials with superior properties. *Ann. Rev. Mater. Res*. 2022;52: 357–382.
7. Liu F, Kirchheim R. Nano-scale grain growth inhibited by reducing grain boundary energy through solute segregation. *J. Cryst. Growth.* 2004;264: 385–391.
8. Chookajorn T, Murdoch HA, Schuh CA. Design of stable nanocrystalline alloys. *Science.* 2012;337: 951–954.
9. Lejček P, Všianská M, Šob M. Recent trends and open questions in grain boundary segregation. *J. Mater. Res*. 2018;33: 2647–2660.
10. Tuchinda N, Schuh CA. Grain size dependencies of intergranular solute segregation in nanocrystalline materials. *Acta Mater*. 2022;226: 117614.
11. Perrin AE, Schuh CA. Stabilized nanocrystalline alloys: The intersection of grain boundary segregation with processing science. *Ann. Rev. Mater. Res*. 2021;51: 241–268.
12. Kim JG, Enikeev NA, Seol JB, Abramova MM, Karavaeva MV, Valiev RZ, Park CG, Kim HS. Superior strength and multiple strengthening mechanisms in nanocrystalline TWIP steel. *Sci. Rep*. 2018;8: 11200.
13. Ke X, Ye J, Pan Z, Geng J, Besser MF, Qu D, Caro A, Marian J, Ott RT, Wang YM, Sansoz F. Ideal maximum strengths and defect-induced softening in nanocrystalline-nanotwinned metals. *Nat. Mater.* 2019;18: 1207–1214.
14. Hu J, Shi YN, Sauvage X, Sha G, Lu K, Grain boundary stability governs hardening and softening in extremely fine nanograined metals. *Science*. 2017;355: 1292–1296.
15. Valiev RZ, Enikeev NA, Murashkin MY, Kazykhanov YU, Sauvage X. On the origin of the extremely high strength of ultrafine-grained Al alloys produced by severe plastic deformation. *Scripta Mater*. 2010;63: 949–952.
16. Chang KI, Hong SI. Effect of sulphur on the strengthening of a Zr-Nb alloy. *J. Nucl. Mater*. 2008;373: 16–21.
17. Sheinerman AG. Strengthening of nanocrystalline alloys by grain boundary segregations. *Mater. Phys. Mech*. 2022;50(2): 193–199.
18. Turlo V, Rupert TJ. Grain boundary complexions and the strength of nanocrystalline metals: Dislocation emission and propagation. *Acta Mater*. 2018;151: 100–111.
19. Pan Z, Sansoz F. Heterogeneous solute segregation suppresses strain localization in nanocrystalline Ag-Ni alloys. *Acta Mater*. 2020;200: 91100.
20. Babicheva RI Bachurin DV, Dmitriev SV, Zhang Y, Kok SW, Bai L, Zhou K. Elastic moduli of nanocrystalline binary Al alloys with Fe, Co, Ti, Mg and Pb alloying elements. *Philos. Mag*. 2016;96: 1598–1612.
21. Babicheva RI, Dmitriev SV, Bachurin DV, Srikanth N, Zhang Y, Kok SW, Zhou K. Effect of grain boundary segregation of Co or Ti on cyclic deformation of aluminium bi-crystals. *Int. J. Fatigue*. 2017; 102: 270–281.
22. Heckman NM, Foiles SM, O'Brien CJ, Chandross M, Barr CM, Argibay N, Hattar K, Lu P, Adams DP, Boyce BL. New nanoscale toughening mechanisms mitigate embrittlement in binary nanocrystalline alloys. *Nanoscale*. 2018;10: 21231.

23. Chiu E, Demkowicz MJ, Srivastava A. Toughening of interface networks through the introduction of weak links. *Acta Mater*. 2021;215: 117090.
24. Molkeri A, Srivastava A, Osovski S, Needleman A. Influence of grain size distribution on ductile intergranular crack growth resistance. *J. Appl. Mech*. 2020;87: 031008.
25. Osovski S, Needleman A, Srivastava A. Intergranular fracture prediction and microstructure design. *Int. J. Fract*. 2019;216: 135–148.
26. Guo X, Chang K, Chen L, Zhou M. Determination of fracture toughness of AZ31 Mg alloy using the cohesive finite element method. *Eng. Fract. Mech*. 2012;96: 401–415.
27. De La Osa MR, Estevez R, Olagnon C, Chevalier J, Tallaron C. Cohesive zone model for intergranular slow crack growth in ceramics: influence of the process and the microstructure. Model. *Simul. Mater. Sci. Eng*. 2011;19: 074009.
28. Abid N, Pro JW, Barthelat F. Fracture mechanics of nacre-like materials using discrete-element models: Effects of microstructure, interfaces and randomness. *J. Mech. Phys. Sol*. 2019;124: 350–365.
29. Pro JW, Barthelat F. Discrete element models of fracture in tooth enamel: Failure mode competition and statistical effects. *J. Mech. Phys. Sol*. 2020;137: 103868.
30. Sheinerman AG. Modeling the effect of grain boundary segregations on the fracture toughness of nanocrystalline and ultrafine-grained alloys. *Metals.* 2023;13: 1295.
31. Kelly PF. *Properties of Materials*. CRC Press; 2014.
32. Xu XP, Needleman A. Numerical simulations of fast crack growth in brittle solids. *J. Mech. Phys. Sol.* 1994;42: 1397–1434.

THE AUTHORS

Sheinerman A.G.
e-mail: asheinerman@gmail.com

Shevchuk R.E.
e-mail: re.shevchuk@gmail.com